Accepted Manuscript

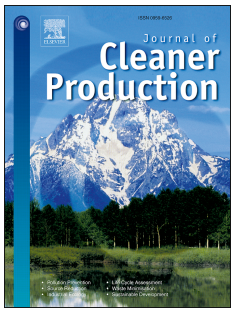

The role of biochar properties in influencing the sorption and desorption of Pb(II), Cd(II) and As(III) in aqueous solution

Eric F. Zama, Yong-Guan Zhu, Brian J. Reid, Gou-Xin Sun

PII: S0959-6526(17)30140-3

DOI: 10.1016/j.jclepro.2017.01.125

Reference: JCLP 8872

To appear in: *Journal of Cleaner Production*

Received Date: 2 September 2016

Revised Date: 19 January 2017

Accepted Date: 21 January 2017

Please cite this article as: Zama EF, Zhu Y-G, Reid BJ, Sun G-X, The role of biochar properties in influencing the sorption and desorption of Pb(II), Cd(II) and As(III) in aqueous solution, *Journal of Cleaner Production* (2017), doi: 10.1016/j.jclepro.2017.01.125.

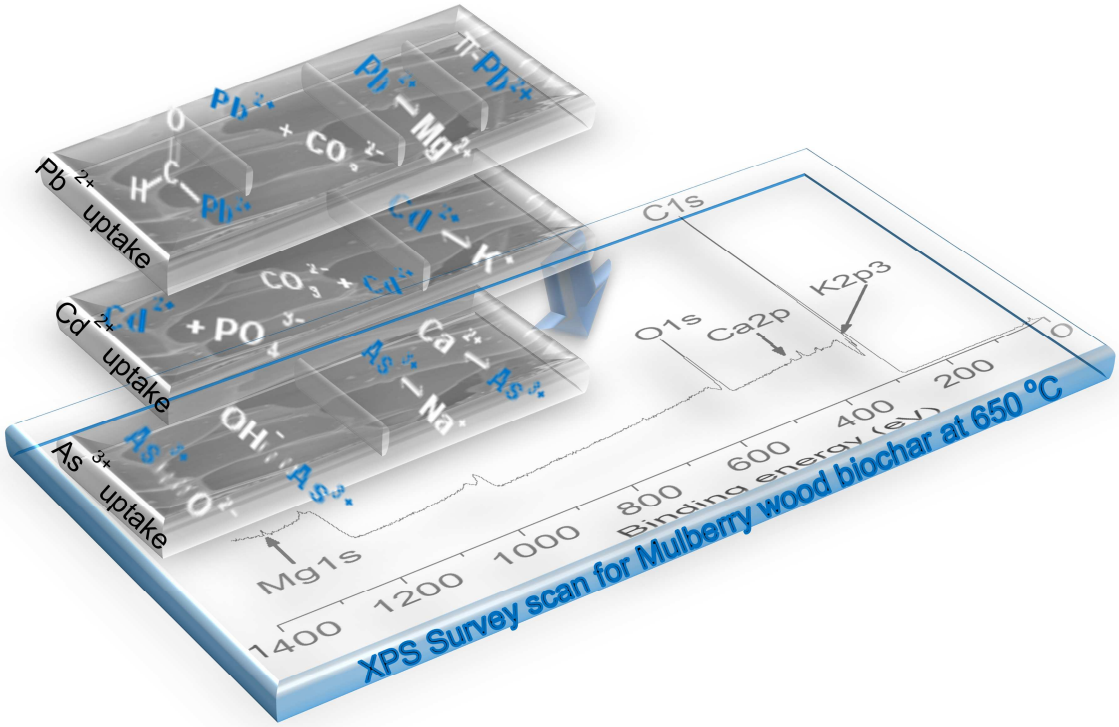

Graphical abstract: Summary of major sorption processes and X-ray photoelectron spectroscopy (XPS) survey scan for mulberry wood biochar at 650 ^{o}C

Wordcount: 5,634 (*not including references and tittle page*)

The role of biochar properties in influencing the sorption and desorption of Pb(II), Cd(II) and As(III) in aqueous solution

Eric F. Zama[!†], Yong-Guan Zhu[!†], Brian J. Reid[^*], Gou-Xin Sun[!*]

[!] State Key Lab of Urban and Regional Ecology, Research Center for Eco-Environmental Sciences, Chinese Academy of Sciences, Beijing 100085, P.R. China

[†] State Key Lab of Urban Environment and Health, Institute of Urban Environment, Chinese Academy of Sciences, Xiamen 361021, P. R. China.

[^] School of Environmental Sciences, University of East Anglia, Norwich Research Park, Norwich NR4 7TJ, UK

***Corresponding author**

Gou-Xin Sun: email; gxsun@rcees.ac.cn , Tel: +86 62849328

Abstract

The chemical and physical properties of 20 biochars produced at 350, 450, 550 and 650 ^{o}C were investigated to determine the key roles they play in the sorption and desorption of three potentially toxic elements (Pb, Cd, As). Biochar surfaces were studied using scanning electron microscopy, Fourier transform infra-red spectroscopy, X-ray diffraction and X-ray photoelectron spectroscopy. Organic functional groups (e.g. –COOH, C=O, C-X), inorganic minerals ($CaCO_3$, SiO_2, $Ca_2Si_5O_{10}\cdot 3H_2O$) and cations ($K^+$, Ca^{2+}, Mg^{2+}, Na^+) controlled PTE sorption significantly while physical properties (morphology, surface area) showed little influence on the sorption of potentially toxic elements. Four major mechanisms accounted for the exceptionally high Pb(II) sorption by all 20 biochars (97.5 - 99.8 %) while Cd(II) and As(III) sorption (< 90 % and 42 % respectively) were controlled by two mechanisms (precipitation and electrostatic attraction) only. Thermodynamic studies suggested that Pb and Cd sorption on a majority of biochars was spontaneous and endothermic while As sorption was also endothermic but not spontaneous. Sorbed PTEs were observed to be very stable over a wide range of pH values (3.5 - 9.5) with desorption ranging from 0.2 - 16.5 %. Detailed understanding of how biochar surface properties interact with PTEs increases the possibility of developing cost effective and engineered biochars with exceptional sorption characteristics.

Key words

Biochar property, Sorption capacity, Potentially toxic element, pH

1. Introduction

As the search for affordable sorbents for potentially toxic elements (PTEs) such as Pb, Cd and As becomes ever more important, biochars and their sorption abilities have been under increasing scientific investigation in recent years. While much has been done to test the sorption abilities of biochar including its redox potential (Saquing et al., 2016), a clearer understanding of the properties of biochar that control its ability to sorb PTEs is yet to be established. Efforts are still being made to understand these surface properties, how they bring changes to biochar sorption behavior and how they can be optimized to enhance PTE sorption.

Biochar is the black, carbon-rich and porous material, obtained by heating any biomass at elevated temperatures (> 250 ^{o}C) under limited oxygen conditions (a process known as pyrolysis) (Tan et al., 2015; Xiao et al., 2016; Yan et al., 2014). During pyrolysis, biomass is known to undergo chemical bond modification leading to dehydration, conversion of aliphatic bonds to aromatic bonds and the consolidation of aromatic bonds into stable graphene (Zhao et al., 2016). The process changes the properties of biochar, and enhances its sorptive capacity for PTEs both in soil and water (Khan et al., 2013; Xiao et al., 2016). Biochar's usefulness in sorbing PTEs has been widely reported (Cernansky et al., 2015; Tan et al., 2015; Xiao et al., 2016) and supported for use to reclaim land contaminated by mining activities by the US environmental protection agency and other companies (Cernansky et al., 2015). Its usefulness extends to soil improvement as it has the ability to immobilize PTEs in soil and also create a favorable environment for soil microbial community (Sun et al., 2008; Sun et al., 2014; Zheng et al., 2013).

PTE sorption onto biochar depends on several factors, such as, the affinity between the PTE and biochar, the specific surface area of biochar exposed to the PTE ions, the concentration of the PTE/biochar in solution, the initial pH of solution as well as the temperature of the system (Chen et al., 2015; Higashikawa et al., 2016; Livingston, 2005). All these factors except temperature may be affected by the surface properties of biochar such as its organic functional groups, structure and porosity, elemental composition, cations exchange capacity (CEC) and the point of zero charge. The surface properties may in turn influence the usefulness of biochar (for remediation purposes) which is determined by the amount of contaminant (PTEs) it can attract and retain under prevailing environmental conditions (Livingston, 2005). During sorption, PTEs often bind strongly to active sites provided by functional groups (e.g. carboxyl, amines, carbonyls, alcoholic and phenolic groups) which have been suggested to have an involvement in PTE complexation (Ahmad et al., 2015; Uchimiya et al., 2012; Vithanage et al., 2015). Other mechanisms of PTE uptake by biochar may include chemical precipitation with inorganic components, coordination with π-electrons (C=C) of carbon, and cationic exchange (Wang et al., 2015).

The sorption abilities of peanut shells (Ps), corn cobs (Cc) poultry manure (Pm), white mulberry wood (Mw) and buckwheat husk (Bw) biochars may have been reported widely (Gai et al., 2014, Yang et al., 2016). However, as far as we know, the key properties of these biochars which govern their effectiveness in removing PTEs from solution (or soil) are still not well understood. The present study focuses on biochar surface properties and their influence on mechanisms driving the sorption of three PTEs (Pb, Cd and As). To introduce a wide spectrum of surface properties, 20 biochars produced from five biomass materials at different temperatures (350, 450, 550 or 650 ^{o}C) were compared. The study lays emphasis on understanding the nature

of surface properties of biochar, how these properties bring changes to biochar sorption abilities and how we might manipulate these properties for better PTE sorption.

2. Materials and Methods

2.1. Reagents, quality control and data analysis

Analytical grade reagents ($PbCl_2$, $CdCl_2 \cdot 2.5H_2O$ and $NaAsO_2$) were used to prepare Pb, Cd and As aqueous solutions, respectively. All samples were dissolved in ultra-pure water (Milli-Q, 18.2 MΩ cm, TOC 3 ppb) to obtain stock solutions that were further diluted to obtain working solutions. All samples in the sorption isotherms tests were prepared in duplicates. Controls were made consisting of biochar only in milli-Q water, PTE only in solution and neither biochar nor PTE in solution. All sorption experiments were carried out at room temperature with initial pH controlled at 5.5 ± 0.2 using 0.1 M HNO_3 or NaOH solutions (Uchimiya, 2014). OriginPro 8.5 (OriginLab, USA), was used for Fourier transform infra-red spectroscopy (FT-IR) and X-ray diffraction (XRD) data analysis and CasaXPS 2.3.17 was used for X-ray photoelectron spectroscopy (XPS) data analysis while sorption and desorption quantities and percentages were calculated using Microsoft excel.

2.2. Biomass and biochar preparation

Biochars used in this study were prepared from five different biomass materials, namely, buckwheat husk-**Bw (***Fagopyrum esculentum)*, corn cobs-**Cc** *(Zea mays)*, mulberry wood-**Mw** *(Morus alba)*, poultry manure-**Pm** and peanut shells-**Ps** *(Arachis hypogae)*. Each biochar was pyrolysed at 4 different temperatures (350, 450, 550 and 650 ^oC) using steel crucibles in a Neytech Muffle Furnace (*Vulcan 3-1750A*) and a near-zero oxygen supply (Agrafioti et al., 2014; Nartey & Zhao, 2014; Woolf et al., 2014). The resulting 20 biochars were coded as

Bw350, Bw450, Bw550, Bw650, Cc350, Cc450, Cc550 etc. During pyrolysis, the temperature was raised at the rate of 10 ^{o}C min^{-1} and maintained at the desired temperature for 4 h. Following pyrolysis, all biochars were allowed to cool to room temperature. They were ground and sieved to obtain a constrained particle size between 0.2 and 0.17 mm.

2.3. Physico-chemical analysis of biochar

The quantity of biochar produced from each biomass material (***yield***) and the quantity of ash produced from each biochar were calculated from equations 1 and 2 (Gai et al., 2014).

$$\% \text{ Yield} = \frac{M_{BC}}{M_{BM}} \times 100 \quad (1)$$

$$\% \text{ Ash} = \frac{M_{ASH}}{M_{BC}} \times 100 \quad (2)$$

Where: M_{BC} = mass of biochar, M_{BM} = mass of biomass, M_{ASH} = mass of ash

Total **C, H, N**, and **S** were measured using an elemental analyzer (Vario EL III) and the O content was calculated on percentage difference basis {i.e. 100 - (%C + %N + %S + %H) = %O} (Wang et al., 2015). The cation exchange capacity (**CEC**) was assessed using the ammonium acetate (NH_4OAc) method (Khan et al., 2013; Robertson et al., 1999) as detailed in *supporting information*. The **pH** of all biochars was measured using a pH meter (Mettler Toledo 320-S) by treating biochar with deionized water in the ratio 1:2. Biochars were examined using a Field Emission Scanning Electron Microscope (**FE-SEM,** SU8000) for structural characterization before and after sorption. The SSA was measured from sorption isotherms at 77 K using the Surface Area and Porosity Analyzer (**ASAP,** 2020 HD88). FT-IR spectroscopic technique was used to determine organic functional groups (OFGs) such as hydroxyls, carboxylates, carbonyls, and amines on the surfaces of the biochars. Thermo Scientific Nicolet FT-IR spectrometer (Nicolet 8700) was used to analyze biochar samples prepared in pellets of fused KBr within the

4000 – 400 cm^{-1} regions. XPS was also used to measure the bonding energies of C, O, N, As, Cd and Pb on the biochars before and after PTE sorption. The ESCALAB 250Xi XPS equipped with monochromatic Al Kα radiation was used to produce survey scans and high resolution scans for C1s, O1s, Pb4f, Cd3d and As3d. To identify mineral crystals in the biochars before and after PTE sorption, an XRD (X'pert Pro, Netherlands) was used equipped with a stepping motor and graphite crystal. A Cu Kα radiation source was used with scans at 2θ in the range 5^0 - 90^0.

2.4. Sorption and desorption tests

Principal stock solutions (30,000 μg L^{-1}) of Pb(II), Cd(II) and As(III) were prepared from $PbCl_2$, $CdCl_2 \cdot 2.5H_2O$ and $NaAsO_2$ respectively. Each stock solution was further diluted to 1,000, 2,000, 3,000, 4,000 and 5,000 μg L^{-1} for initial PTE solution concentrations in the sorption tests. These low initial concentrations were intended to simulate the typical concentration of these contaminants in water (or soil). Nazir et al. (2015) observed that the average concentration of these PTEs in most soils and water in China fall within the chosen range. All solutions were prepared with a background electrolyte of 0.01 M $NaNO_3$ to maintain ionic strength (Biswal & Paria 2010, Mir 2010).

Sorption experiments were conducted by adding 0.05 g of biochar to 10 mL of Pb(II), Cd(II) or As(III) solutions. Before adding biochar the pH of the PTE solutions was adjusted to 5.5 ± 0.2 by adding 0.1 M HNO_3 or NaOH solutions (Uchimiya, 2014). Desorption experiments were carried out using 0.05 g (dry mass) of PTE-loaded biochar and 10 mL of electrolyte solutions made at pH 3.5, 5.5, 7.5 and 9.5. ICP-MS (7500a, Agilent Technologies, USA) was used to determine the concentrations of PTEs in solutions after sorption and desorption. Details of the methods in sorption and desorption tests and sorption models (Langmuir and Freundlich models) are presented in *supporting information.* Acid demineralization of biochars was done by treating

1 g of biochar with 100 mL of 1 M HCl solution as described by Wang et al. (2015). All sorption and desorption experiments were carried out in duplicate.

Thermodynamic parameters including Gibbs free energy change (ΔG^o), enthalpy change (ΔH^o), and entropy change (ΔS^o) for Pb, Cd and As sorption on biochars were estimated from equations 3 and 4 (Liu, 2009). All biochars pyrolysed at 350 and 650 ^oC were used in this experiment with solution temperatures ranging from 25 - 45 ^oC (298 – 318 K) while other parameters like pH were kept constant.

$$\Delta G^o = - RT \, \mathrm{Ln} K_C \quad (3)$$

$$\Delta G^o = \Delta H^o - T\Delta S^o \quad (4)$$

*Where: R = the universal gas constant (*8.314 J mol^{-1} K^{-1}*), K_C = thermodynamic constant, T = temperature (K)*

K_C is dimensionless and obtained by multiplying the Langmuir equilibrium constant (K_L) (*supporting information*) by 55.5 (moles of water per liter of solution). A linear plot of ΔG^o versus T in equation 4 gives values of ΔH^o and ΔS^o from the intercept and slopes respectively (Liu, 2009).

3. Results and Discussion

3.1. Changes in biochar properties with changing pyrolysis temperature

As pyrolysis temperature increased from 350 to 650 ^oC, significant changes occurred both in the chemical and physical structure of the biochars as confirmed by changes in the elemental content (**Table 1**), changes in organic functional groups (FT-IR analysis-**Fig. 1** and XPS analysis-**Fig. 2**) and changes in the concentration and occurrence of inorganic mineral components (CO_3^{2-}, PO_4^{3-}, SO_4^{2-}) and cations (Al^{3+}, Ca^{2+}, Mg^{2+}, Na^{+}). Pyrolysis temperature is therefore a key determinant of the physical and chemical properties of biochar which in turn,

have a strong effect on their sorptive capacities (Jiang & Wang, 2016; Fang et al., 2013; Xiao et al., 2014).

3.1.1. Changes in elemental content

While carbon content increased with increasing pyrolysis temperature (**Fig. S1**), biochar yield decreased as temperature increased from 350 ^{o}C to 650 ^{o}C (**Table 1**). Similar studies have attributed decrease in biochar yield to dehydration and the loss of volatile matter and non-condensable gases such as CO_2, CO, H_2 and CH_4 (Ahmad et al., 2014; Gai et al., 2014; Tan et al., 2015) while carbon content increased because of increasing carbonization at higher temperatures (Ahmad et al., 2014). During pyrolysis, increase in temperature causes biomass to undergo thermochemical decomposition with the formation of stronger and more resistant graphitic bonds as hemicellulose, cellulose and lignin break down completely (Ahmad et al., 2014; Tan et al., 2015). Biochar yield from poultry manure (Pm) was significantly higher (60 - 80 %) than other biochars (21 - 56 %) with a relatively very low carbon content (23 - 24 %) compared to other biochars (50 - 83 %) (**Fig. S1**). This may be due to (i) the inability of Pm to undergo depolymerization due to lack of lignocellulosic compounds and (ii) the presence of inorganic compounds such as Zn, P, Si, Mg, and K (Ahmad et al., 2014). High inorganic mineral content observed for Pm is supported by a relatively higher CEC (33.2 - 47.9 $cmol_c\ kg^{-1}$) and ash content (71 - 79 %) compared to other biochars which ranged from 10.1 - 23.3 $cmol_c\ kg^{-1}$ and 4 - 44 %, respectively (**Table S2**). The contents of C, H, N, S and O in biochars are indicators of carbonization, hydrophobicity and polarity of the biochar. Hydrogen and Oxygen contents with their associated atomic ratios (H:C, O:C, and (O+N):C) decreased with increasing temperatures for all biochars (**Table S2**). This decrease suggested dehydration and deoxygenation of biomass with increasing temperatures (Ahmad et al., 2014). This means that the biochars became less

hydrophilic with weaker polar groups as pyrolysis temperatures increased. Apart from C, H, O, N and S, mineral elements (Mg, Ca, K and P) on the biochars surfaces were also determined by XPS analysis on Mw, Ps and Bw at 350 and 650 ^{o}C. Survey scans for Mw350 and Mw650 are shown in **Fig. 2a** and **2b** while scans for the rest of the biochars can be seen in *supporting information* (**Fig. S7**). Most of these minerals were scattered on the surfaces of the biochars with high concentrations on biochars pyrolysed at higher temperatures due to increasing ash content (Yang et al., 2016).

3.1.2. Changes in organic functional groups (OFGs)

OFGs on the surfaces of biochar develop during pyrolysis, 'involving the cleavage of O-alkylated carbons and anomeric O-C-O carbons in addition to the production of fused-ring aromatic structures and aromatic C-O groups (Li et al., 2013). FT-IR analysis on all 20 biochars indicated broad peaks between 3300 and 3240 cm^{-1} (**Fig. 1**) corresponding to O-H bond stretching in alcohols and phenols (Trigoa et al., 2016; Wade, 2013). These bands greatly weakened or disappeared at higher pyrolysis temperatures (650 ^{o}C). Major bands also occurred between 2962 cm^{-1} and 2823 cm^{-1} which correspond to the vibrations of strong C-H bond in methyl, alkanes or aldehydes (Wade, 2013). These results were confirmed by XPS analysis which showed a strong peak at 284.7 eV on Mw350 and Mw650 corresponding to C-H, C-C and C=C functional groups (**Figs. 2a, 2b insets).** All the biochars except Pm350, Pm450, Pm550, Pm650 and Mw650, showed FT-IR peaks between 1600 - 1250 cm^{-1} (**Fig. 1**) which corresponds to esters and aromatic C=C or C=O stretches in carboxylates (Chen et al., 2015). Most of these bands also greatly dwindled or disappeared at higher temperatures (> 550 ^{o}C) as C=O easily ruptures to form gases and liquids while esters give way for the development of lactones (Chen et al., 2015; Chun et al., 2004; Yang et al., 2016). These results were also consistent with XPS

analysis on Mw350 which returned a peak at 287.9 eV corresponding to C=O functional group (**Fig. 2a inset**). At higher temperatures (650 ^{o}C), the peak shifted to 288.1 eV (**Fig. 2b inset**) corresponding to C=O, C-F, O=C-OH or O=C-NH (Fang et al., 2013). Other significant bands on the FT-IR spectrum occurred around 1095, 787, and 509 cm^{-1} (**Fig. 1**) representing ordinary C-X stretching of halides or C-N stretches of aliphatic amines and strong C-H stretches of trisubstituted alkenes respectively (Wade, 2013). Again, XPS analysis confirmed these results with a peak at 293.3 eV for Mw350 which shifted to 293.4 eV in Mw650 all representing C-F_3 groups (**Fig. 2a and 2b insets** respectively). The occurrence of fluorine on Mw at higher temperature was unexpected but may have originated from the parent material.

3.1.3. Changes in cation exchange capacity (CEC)

The CEC, which slightly decreased with increasing temperatures, varied among biochars from different biomass materials but did not vary significantly among biochars from the same biomass materials (**Table 1**). Bw had the lowest CEC ranging from 10.1 $cmol_c$ kg^{-1} in Bw550 to 11.7 $cmol_c$ kg^{-1} in Bw650 (**Table 1**). Pm had the largest CEC ranging from 33.2 $cmol_c$ kg^{-1} in Pm650 to 47.9 $cmol_c$ kg^{-1} in Pm350 (**Table S2**). The large CEC for Pm could be attributed to the large amounts of inorganic minerals often added to poultry feed.

3.1.4. Changes in morphology/specific surface area (SSA)

There was a significant increase in porosity of the biochars as they passed from 350 ^{o}C to 650 ^{o}C (**Fig. S4**). The specific surface area (SSA) for most of the biochars also increased with increasing pyrolysis temperature ranging from 11.4 m^2 g^{-1} – 58.0 m^2 g^{-1} in Bw350 and Mw550 respectively (**Table 1**). The breakdown of aliphatic bonds and their gradual conversion to aromatic linkages with planar sheets of graphene as temperature rises from 350 to 650 ^{o}C may be responsible for the increase in SSA of the biochars (Sorrentia et al., 2016; Tan et al., 2015). The

SSA for Pm at all temperatures was relatively very small ranging from 3.33 $m^2 g^{-1}$ - 8.97 $m^2 g^{-1}$ in Pm350 and Pm550 respectively (**Table S2**). This could be attributed to the lack of lignocellulosic compounds in Pm and the presence of large amounts of inorganic minerals (e.g. Zn, P, Si, Mg, and K) which reduce porosity during pyrolysis (Tan et al., 2015; Xu et al., 2013). Pore number, pore size and pore volume often correlate positively with SSA of biochar with increase in these factors leading to increase in SSA of biochar (Nartey and Zhao, 2014; Tan et al., 2015).

3.2. The influence of biochar properties on PTE sorption

3.2.1. Pb(II) sorption

Pb(II) sorption on all biochars was exceptionally high (> 97.5 %) (**Fig. S2**). This could be attributed to 4 main biochar properties: (i) organic functional groups, (ii) mineral content, (iii) ionic content and (iv) π-electrons.

Organic functional groups (e.g. C-H, –COOH, –OH, C=O and C-X) on the surfaces of biochars were detected by FT-IR and XPS analysis. Following Pb sorption on Mw350 and Mw650, deconvulated C1s scans showed few new peaks at 286.2 eV and 286.1 eV respectively (**Figs. 2c, 2d**) corresponding to C-O, C-OH, and C-O-C functional groups (Fang et al., 2013). The occurrence of fewer peaks suggested that most functional groups were used up in complexation reactions with Pb(II). This was confirmed when biochar was de-mineralized by an acid dipping method (Yang et al., 2016) and after equilibration, a drop in solution pH from the standard 5.5 to 3.8 on average confirmed that complexation processes, which often release H^+, took place during Pb(II) sorption. FT-IR analysis on Pm in particular, returned the smallest number of peaks (3 on average) at all temperatures suggesting that limited polar groups were involved in complexation reactions on the biochar. However a high sorption capacity for Pb on

Pm was likely due to high ionic exchange and chemical precipitation resulting from its large ionic content (Liu et al., 2016).

Inorganic minerals on the surfaces of biochars were identified by XRD analysis. Results are presented on **Fig. 3**. Crystalline calcite ($CaCO_3$), Quartz (SiO_2) and Gonnardite [$(Na, Ca)_2$ $(Si, Al)_5O_{10}\cdot 3H_2O$] were the main inorganic minerals detected on biochars before PTE sorption (**Fig. 3a**). These minerals released anions (e.g. CO_3^{2-}, and PO_4^{3-}) which bond with Pb(II) to form precipitates (Yang et al., 2016). Post-sorption XRD patterns of Mw, Ps and Bw at 350 and 650 ^oC indicated peaks at 25^o, 28^o, 30^o, 31^o, and 38^o (**Fig. 3b**) corresponding to $PbCO_3$, $PbCO_3(OH)_2$, $Pb_3(PO_4)_2$, $Pb_9(PO_4)_6$, and $Pb_3(CO_3)_2(OH)_2$ respectively (Xu et al., 2013). This large amount of mineral precipitates suggested that precipitation was the main mechanism driving Pb sorption. XPS spectra (Pb4f scans) on biochars after Pb sorption also showed peaks at 139.4 eV for Mw350 indicating the deposition of $PbSO_4$ (**Fig. 2c inset**). At higher temperatures (650 ^oC) this peak shifted to 139.0 eV (**Fig. 2d inset**) indicating the presence of $PbCl_2$ (Liu et al., 2016). FT-IR analysis of the post-sorption biochars also suggested the presence of precipitates with bond stretches appearing at lower frequencies (< 1400 cm^{-1}) corresponding to PO_4^{3-} and CO_3^{2-} (Pb^{2+}-phosphate or carbonate precipitation) (Yang et al., 2016).

Coordination with delocalized π-electrons (e.g. C=C, C=O) may have also played a role in Pb(II) sorption. Many more bond stretches appearing around 1500 cm^{-1} and 1400 cm^{-1} after Pb(II) sorption (**Fig. 1b**) was equally an indication that Pb^{2+}-π-electrons interaction took place during sorption.

The above results suggest that at least four sorption mechanisms driven by four main biochar properties were responsible for Pb(II) sorption on the biochars. These sorption mechanisms may have taken place simultaneously or supplementing each other. Similar studies also suggested that

chemical precipitation with inorganic components was the dominant mechanism responsible for Pb(II) uptake on Ps (Inyang et al., 2012; Liu et al., 2016; Wang et al., 2015;).

3.2.2. Cd(II) sorption

Cd(II) sorption mainly ranged between 50 and 90 % (**Fig. S2**). There was no evidence of complexation reactions during Cd(II) sorption. Unlike Pb(II) sorption where solution pH decreased after de-mineralizing biochar using the acid dipping method, there was no significant drop in solution pH after Cd(II) sorption suggesting that functional groups did not play any significant role in Cd(II) sorption. After Cd(II) sorption, XRD patterns of Mw, Ps and Bw at 350 and 650 ^{o}C showed peaks around 32^{o}, and 41^{o} (**Fig. 3c**) corresponding to $Cd_9(PO_4)_6$ and $CdCO_3$ (Otavite) respectively (Liu et al., 2016). The presence of these precipitates was evidence that mineral ions played a role in Cd(II) sorption. Similar studies have also attributed Cd(II) sorption to surface precipitation by the formation of insoluble cadmium compounds in alkaline condition, and also ion exchange with exchangeable cations in the biochar (Chen et al., 2015; Uchimiya, 2014).

3.2.3. As(III) sorption

The uptake of As(III) was < 42 % on all biochars especially Mw. Like Cd(II) sorption, de-mineralized biochar equilibrated with As(III) did not show any significant drop in solution pH, suggesting that functional groups did not play any role in As(III) uptake. XRD analysis on Mw, Ps and Bw after As(III) sorption did not show any new peaks (**Fig. 3d**) which was confirmation that mineral ions did not interact significantly with As(III). Similar studies have ascribed As(III) sorption to weak electrostatic attraction and ion exchange which may confirm why As(III) sorption was the weakest in this study (Liu et al., 2016).

Throughout the study, there was no significant evidence that physical sorption took place between biochars and PTEs. This was supported by the relatively poor correlation between the SSA of biochars and sorption capacities.

3.2.4. Effects of initial solution concentration on PTE sorption

Results of the effects of initial solution concentration on PTE sorption at 350 and 650 ^{o}C are presented on **Fig. 4**. Complete results can be seen in *supporting information* (**Fig. S6**). The percentage of PTE removed from solution decreased as a function of the initial amount of PTE added to solution. This decrease could be ascribed to the ratio of solute (PTE) in solution to the available sorption sites. At lower initial concentration, this ratio is lower which influences PTE uptake but at higher initial PTE concentration, the ratio is higher and the available sorption site quickly becomes saturated which decreases PTE uptake (Okeola et al., 2012). Similar results were reported by Mohanty and Boehm (2014) while working on *E. coli* removal by biochar. Pb sorption on Cc at all temperatures dropped significantly at higher solution concentrations while its sorption on Bw, Mw, Pm and Ps did not vary considerably across the five solution concentrations (1,000, 2,000, 3,000, 4,000, and 5,000 µg L^{-1}) (**Fig. 4**). This implies that while initial solution concentration does not greatly affect Pb sorption on Bw, Mw, Pm and Ps, lower concentrations are preferable for its sorption on Cc. For Cd, solution concentration did not significantly influence its sorption by Ps especially at 350 ^{o}C and 450 ^{o}C. However solution concentration significantly influenced the sorption of Cd on Bw, Cc, Mw and Pm with sorption amounts varying considerably as temperatures increased from 350 – 650 ^{o}C (**Fig. 4**). Most of the biochars had similar sorption behaviors on As(III) when temperatures increased from 350 – 650 ^{o}C and across the five solution concentrations. However Mw had the least sorption capacity for As(III), which varied considerably as temperatures increased from 350 – 650 ^{o}C. The removal of

As(III) by Pm at lower temperatures and lower concentrations was poor but at higher temperatures, the performance of this biochar was relatively good even at lower concentrations.

4. Sorption characteristics

4.1. Sorption capacities

The effective removal of Pb(II), Cd(II) and As(III) from solution by biochars was expressed in terms of percentage (%) removal and maximum sorption capacity (Q_{max}) calculated from the Langmuir model (*equation S2*). Q_{max} values for all 20 biochars are shown on **Fig. 5** while % removal is shown in *supporting information* (**Fig. S2**). All biochars significantly removed Pb(II) from solution with Q_{max} ranging from 1,101 to 2,500 µg g^{-1} (97.5 - 99.8 %). The Q_{max} of Cd(II) mainly ranged between 68 to 1,666 µg g^{-1} (50 - 70 %) while As(III) was least sorbed (2 - 588 µg g^{-1}) (< 42 %). The attraction between biochar and PTE (affinity) is often represented by the Langmuir and Freundlich intensity constants K_L and 1/n respectively. In this study, the sorption processes of Pb(II), Cd(II), and As(III) on all biochars were favorable with values of 1/n ranging between 0.1 and 1 (**Table S1**).

4.2. Sorption thermodynamics

Calculated changes in Gibbs free energy (ΔG^o), enthalpy (ΔH^o), and entropy (ΔS^o) for the sorption of Pb(II), Cd(II) and As(III) on biochars are shown in Table 2. Additional thermodynamics information is presented in *supporting information* (Table S3). The sorption of Pb(II) on all biochars was feasible and spontaneous as indicated by negative ΔG^o values (Table 2) while positive and negative values of ΔH^o and ΔS^o respectively (Table 2) suggested an endothermic and less chaotic (random) sorption process at the solid-solution interface (Kizito et al., 2015; Moyo et al., 2016). The sorption of Cd(II) on a majority of biochars was feasible, spontaneous, endothermic and less chaotic (Table S3) while As(III) sorption was not feasible and

353 spontaneous on any of the biochars as indicated by positive ΔG^o values. This result may also
354 explain why the sorption capacity of As(III) on all biochars was very low (< 42 %). Like Pb(II)
355 and Cd(II), the sorption of As(III) on a majority of the biochars was endothermic with lesser
356 movements at the solid-solution interface as indicated by positive ΔH^o values and negative ΔS^o
357 values respectively (Table S3). Pb(II) sorption on all biochars was favored at higher temperatures
358 as the negativity of ΔG^o values increased with increasing temperatures (Table 2) (Moyo et al.,
359 2016). Higher temperatures did not favour Cd(II) sorption on a majority of the biochars as ΔG^o
360 decreased with increasing solution temperatures while As(III) sorption did not show any clear
361 dependency on solution temperature (Table S3)

362 **4.3. Sorption isotherms and models**

363 **Fig. S3** shows isotherm curves for all biochars at 350, 450, 550 and 650 ^oC. Isotherms are
364 used to describe 'the relationship between the concentration of solute in solution and the quantity
365 sorbed at the solid phase at constant temperature' (Livingston, 2005). Based on isotherms and
366 Q_{max} values of the biochars, the most effective and least effective were:

367 **Pb**: Mw550>Mw350>Mw450>……>Ps350>Ps550>Cc350

368 **Cd**: Ps350>Ps550>Ps450>……>Cc350>Pm650>Bw350

369 **As**: Bw450>Cc450> Bw350>……>Pm350>Mw350>Mw450

370 Two isotherm models (Langmuir and Freundlich) were used to fit the data. Based on R^2
371 values obtained from linear curves of the Langmuir and Freundlich models (**Table S1**), Pb
372 sorption on all biochars was best fitted using the Freundlich isotherm model (R^2 = 0.88 - 0.99)
373 than the Langmuir model (R^2 = 0.77 - 0.98). This implies that lead sorption was characterized by
374 heterogeneous multilayer sorption with a distribution of sorption sites of different characteristic
375 energies. The Langmuir model provided a good fit to the sorption data of Cd on Bw, Cc, and Mw

at all temperatures (R^2 = 0.72 - 0.99) while the Freundlich model provided a better fit to the sorption data of Cd on Pm and Ps (R^2 = 0.93 - 0.99). The Langmuir model assumes a monolayer sorption on a finite number of sites with homogeneous energy distribution where sorbed particles have no mutual interaction (Zhou et al., 2013). For As, the sorption data on 14 biochars were best fitted using the Langmuir model (R^2 = 0.60 - 0.99) while the Freundlich model provided a better fitting for 6 biochars (R^2 = 0.86 - 0.96) (**Table S1**). There was at least one biochar (Mw650) where neither Langmuir nor Freundlich models fitted its sorption data for arsenic (R^2 = 0.60 and 0.29 respectively) while both Langmuir and Freundlich models (R^2 = 0.99 and 0.99 respectively) provided good fits to the sorption data of some PTEs like Pb on Bw350. This suggests both monolayer and multilayer sorption processes were taking place under the test conditions.

4.4. PTE desorption and effects of pH

Following sorption, the stability of PTEs on biochar was tested in desorption experiments. Bw, Mw and Ps at 450 and 550 ^{o}C were used and the pH was varied at 3.5, 5.5, 7.5 and 9.5. Results indicated that PTE desorption decreased with increasing pH from 3.5 to 9.5 (**Fig. 6**). Pb was the most stable PTE with a maximum percentage desorption of 0.9 % on Mw550 whereas Cd was the least stable PTE with a maximum percentage desorption of 16.5 % on Ps550 (**Fig. 6**). While Pb was more stable on Mw450 than Mw550, Cd and As were more stable on Ps550 and Bw550 than Ps450 and Bw450 respectively. However with a maximum percentage desorption of 16.5 % for all the tested biochars, sorbed PTEs were considered very stable on the biochars over a wide range of pH values.

5. Conclusions

A deeper understanding of the properties of biochar that control its ability to sorb PTEs is promising for the development of cost effective and engineered biochar composites with superior sorption qualities in soil/water remediation programs. The surface properties of biochars produced from buck wheat, corn cobs, mulberry wood, poultry manure and peanut shells at 350, 450, 550 and 650 ^{o}C, have a direct influence on sorption mechanisms which in turn determine the sorption capacities of biochars. Pb sorption on biochars is controlled by multiple sorption mechanisms while Cd and As sorption is controlled by two sorption mechanisms only. Maintaining the pH of media (water or soil) at higher pH values is crucial in retaining sorbed PTEs on biochars. When the pH is reduced, the stability of the sorbed PTEs may be compromised leading to increased desorption.

Acknowledgements

This project was financially supported by the National High Technology Research and Development Program of China (863 Program, 2013AA06A209), Natural Science Foundation of China (No. 41371459), the State Key Program of Natural Science Foundation of China (No. 41330853 &41430858) and CAS-TWAS President's fellowship.

References

Agrafioti, E.; Kalderis, D.; Diamadopoulos, E. Arsenic and chromium removal from water using biochars derived from rice husk , organic solid wastes and sewage sludge, *J. Environ. Manage*. **2014**, 133, 309–314.

420 Ahmad, M.; Rajapaksha, A. U.; Lim, J. E.; Zhang, M.; Bolan, N.; Mohan, D.; Vithanage, M.;
421 Lee, S. S.; Ok, Y. S. Biochar as a sorbent for contaminant management in soil and water: A
422 review. *Chemosphere*, **2014**, 99, 19–23.
423 Biswal, N. R.; Paria, S. Effect of electrolyte solutions on the adsorption of surfactants at PTFE−
424 water interface. *Ind. Eng. Chem. Res.*, **2010**, 49, 7060–7067
425 Cernansky, R. Agriculture: State-of-the-art soil; a charcoal-rich product called biochar could
426 boost agricultural yields and control pollution. Scientists are putting the trendy substance to
427 the test. *Nature News*, **2015**, 517, 258–260.
428 Chen, T.; Zhou, Z.; Han, R.; Meng, R.; Wang, H.; Lu, W. Adsorption of cadmium by biochar
429 derived from municipal sewage sludge: Impact factors and adsorption mechanism.
430 *Chemosphere*, **2015**, 134, 286–293.
431 Chun, Y.; Sheng, G.; Chiou, C.; Xing B. Compositions and sorptive properties of crop residue-
432 derived chars. *Environ. Sci. Technol*. **2004**, 38, 4649-4655.
433 Fang, Q.; Chen, B.; Lin, Y.; Guan Y. Aromatic and hydrophobic surfaces of wood-derived
434 biochar enhance perchlorate adsorption via hydrogen bonding to oxygen-containing organic
435 groups. *Environ. Sci. Technol.* **2013**, 48, 279−288.
436 Gai, X.; Wang, H.; Liu, J.; Zhai, L.; Liu, S.; Ren, T.; Liu, H. Effects of feedstock and pyrolysis
437 temperature on biochar adsorption of ammonium and nitrate. *PLoS ONE*, **2014**, 9, e113888
438 Higashikawa, F. S.; Conz, R. F.; Colzato, M.; Cerri, C. E. P.; Alleoni, L. R. F. Effects of
439 feedstock type and slow pyrolysis temperature in the production of biochars on the removal
440 of cadmium and nickel from water. *J. Clean. Prod.* **2016**, 137, 965–972

441 Inyang, M.; Gao, B.; Yao, Y.; Xue, Y.; Zimmerman, A; Pullammanappallil, P.; Cao, X. Removal
442 of heavy metals from aqueous solution by biochars derived from anaerobically digested
443 biomass. *Bioresource Technol*. **2012**, 110, 50-56
444 Khan, S.; Chao,C.; Waqas, M.; Arp, H. P.; Zhu, Y. G. Sewage sludge biochar influence upon
445 rice (*Oryza sativa*) yield, metal bioaccumulation and greenhouse gas emissions from acidic
446 paddy soil. *Environ. Sci. Technol.*, **2013**, 47, 8624–8632.
447 Kizito S.; Wu, S.; Kirui, W. K.; Lei, M.; Lu, Q.; Bah, H.; Dong, R. Evaluation of slow pyrolyzed
448 wood and rice husks biochar for adsorption of ammonium nitrogen from piggery manure
449 anaerobic digestate slurry. *Sci. Total Environ.* **2015**, 505, 102–112
450 Li, X.; Shen, Q.; Zhang, D.; Mei, X.; Ran, W. Xu,Y.; Yu, G. Functional groups determine
451 biochar properties (pH and EC) as studied by two-dimensional ^{13}C NMR correlation
452 Spectroscopy. *PLoS ONE*. **2013**, 8, e065949
453 Liu, X.; Ding, H.; Wang, Y.; Liu, W.; Jiang, H. Pyrolytic temperature dependent and ash
454 catalyzed formation of sludge char with ultra-high adsorption to 1-Naphthol. *Environ. Sci.*
455 *Technol.*, **2016**, 50, 2602–2609
456 Liu, Y. Is the free energy change of adsorption correctly calculated? *J. Chem. Eng.* **2009**, 54,
457 1981–1985
458 Livingston J. V., Ed. *Trends in water pollution research*. Nova Science publishers: New York,
459 **2005**.
460 Mir, S. Effect of electrolytes on the adsorption of nitrite and nitrate from aqueous solutions by
461 activated carbon. *J. Appl. Sci. Environ.* **2010**, 14, 5–11.

462 Mohanty, S. K.; Boehm A. B. *Escherichia coli* removal in biochar-augmented biofilter: effect of
463 infiltration rate, initial bacterial concentration, biochar particle size, and presence of compost.
464 *Environ. Sci. Technol.*, **2014**, 48, 11535–11542
465 Moyo, M.; Lindiwe, S. T.; Sebata, E.; Nyamunda, B. C.; Guyo, U. Equilibrium, kinetic, and
466 thermodynamic studies on biosorption of Cd(II) from aqueous solution by biochar. *Res.*
467 *Chem. Intermed.*, **2016**, 42, 1349-1362.
468 Nartey, O; Zhao B. Biochar preparation, characterization and adsorptive capacity and its effects
469 on bioavailability of contaminants: An overview. *Adv. Mat. Sci. Eng.* **2014**, 1687-8442
470 Nazir, R.; Khan, M.; Masab, M.; Rehman, H; Rauf, N. Accumulation of heavy metals (Ni, Cu,
471 Cd, Cr, Pb, Zn, Fe) in the soil, water and plants and analysis of physico-chemical parameters
472 of soil and water collected from Tanda Dam kohat. *J. Pharm. Sci. Res.* **2015**, 7, 89-97.
473 Okeola, O; Odebunmi, E.; Ameen O. Comparison of sorption capacity and surface area of
474 activated carbon prepared from *Jatropha curcas* fruit pericarp and seed coat. *Bull. Chem.*
475 *Soc.* **2012**, 26, 171-180.
476 Robertson, G.; Coleman, D.; Bledsoe, C.; Sollins P.; Eds. Standard soil methods for long term
477 ecological research, *Oxford University Press*: New York,**1999**
478 Saquing J. M.; Yu, Y.H.; Chiu P.C. Wood-derived black carbon (biochar) as a microbial electron
479 donor and acceptor. *Environ. Sci. Technol. Lett.*, **2016**, 3, 62–66
480 Sorrentia, G.; Masiellob, C. A.; Duganc, B.; Toselli, M. Biochar physico-chemical properties as
481 affected by environmental exposure. *Sci. Total Environ.* **2016**, 563–564, 1, 237–246
482 Trigoa, C.; Coxb, L.; Spokas, K. Influence of pyrolysis temperature and hardwood species on
483 resulting biochar properties and their effect on azimsulfuron sorption as compared to other
484 sorbents. *Sci. Total Environ.* **2016**, 566–567, 1454–1464

485 Sun, G.X.; Williams, P. N.; Carey, A. M.; Zhu, Y. G.; Deacon, C.; Raab, A.; Feldmann J.; Islam,
486 R. M.; Meharg. A. A. Inorganic arsenic in rice bran and its products are an order of
487 magnitude higher than in bulk grain. *Environ. Sci. Technol.*, **2008**, 42, 7542–7546
488 Sun, Y.; Gao, B.; Yao, Y.; Fang, J.; Zhang, M.; Zhou, Y. Chen, H.; Yang, L. Effects of feedstock
489 type, production method, and pyrolysis temperature on biochar and hydrochar properties.
490 *Chem. Eng. J.* **2014**, 240, 574–578.
491 Tan, X.; Liu, Y.; Zeng, G.; Wang, X.; Hu, X.; Gu, Y.; Yang, Z. Application of biochar for the
492 removal of pollutants from aqueous solutions. *Chemosphere.* **2015**, 125, 70-85.
493 Uchimiya, M. Influence of pH, ionic strength, and multidentate ligand on the interaction of Cd
494 with biochars. ACS *Sustain. Chem. Eng.* **2014**, 4, 2019–2027
495 Uchimiya, M.; Bannon, D.; Wartelle, L. Retention of heavy metals by carboxyl functional
496 groups of biochars in small arms range soil. *J. Agric. Food Chem.* **2012**, 60, 1798−1809.
497 Vithanage, M.; Rajapaksha, A.; Ahmad, M.; Uchimiya, M.; Dou, X.; Alessi, D.; Ok, Y. S.
498 Mechanisms of antimony adsorption onto soybean stover-derived biochar in aqueous
499 solutions. *J. Environ. Manage*. **2015**, 151, 443–449.
500 Wade, Jr. L. G., Organic Chemistry. *Pearson Education, Inc*: 8th, ed. USA., **2013**.
501 Wang, S.; Gao, B.; Zimmerman, A.; Li, Y.; Ma, L.; Harris, W.; Migliaccio, K.W.
502 Physicochemical and sorptive properties of biochars derived from woody and herbaceous
503 biomass. *Chemosphere*. **2015**, 134, 257–262.
504 Woolf, D.; Lehmann, J.; Fisher, E.; Angenent, L. Biofuels from pyrolysis in perspective: Trade-
505 offs between energy yields and soil-carbon additions. *Environ. Sci. Technol.* **2014**, 48, 6492-
506 6499.

Xiao, X.; Chen, Z.; Chen, B. H/C atomic ratio as a smart linkage between pyrolytic temperatures, aromatic clusters and sorption properties of biochars derived from diverse precursory materials. *Sci. Rep.*, **2016**, 6, 22644

Xiao, X.; Chen, B.; Zhu, L. Transformation, morphology, and dissolution of silicon and carbon in rice straw-derived biochars under different pyrolytic temperatures. *Environ. Sci. Technol.* **2014**, 48, 3411-3419.

Xu, X.; Cao, X.; Zhao, L. Comparison of rice husk- and dairy manure-derived biochars for simultaneously removing heavy metals from aqueous solutions: Role of mineral components in biochars. *Chemosphere*, **2013**, 92, 955–961

Xu, X.; Cao, X.; Zhao, L.; Wang, H. Removal of Cu, Zn, and Cd from aqueous solutions by the dairy manure-derived biochar. *Environ. Sci. Pollut. Res.* **2013**, 20, 358–368.

Yan, L.; Kong, L.; Qu, Z.; Li, L.; Shen, G. Magnetic biochar decorated with ZnS nanocrystals for Pb (II) removal. *ACS Sustain. Chem. Eng.* **2014**, 3, 125-132.

Yang, F.; Zhao, L.; Gao B.; Xu, X.; Cao, X. The interfacial behavior between biochar and soil minerals and its effect on biochar stability. *Environ. Sci. Technol.*, **2016,** 50, 2264–2271.

Zhang, J.; Wang, Q. Sustainable mechanisms of biochar derived from brewers' spent grain and sewage sludge for ammonia–nitrogen capture. *J. Clean. Prod.* **2016**, 112, 3927–3934

Zhao, L.; Cao, X.; Zheng, W.; Scott, J. W.; Sharma, B. K.; Chen, X. Copyrolysis of biomass with phosphate fertilizers to improve biochar carbon retention, slow nutrient release, and stabilize heavy metals in soil. *ACS Sustain. Chem. Eng.* **2016**, 4, 1630–1636

Zheng, R.; Chen, Z.; Cai, C.; Wang, X.; Huang, Y.; Xiao, B.; Sun G. Effect of biochars from rice husk, bran and straw on heavy metal uptake by pot-grown wheat seedling in a historically contaminated soil. *BioResources*. **2013**, 8, 5965-5982

530 Zhou, Y.; Gao, B.; Zimmerman, A. R.; Fang, J.; Sun, Y.; Cao, X. Sorption of heavy metals on
531 chitosan-modified biochars and its biological effects. *Chem. Eng. J*, **2013**, 231, 512–518.
532

533 # Tables

534 # Tables

535 **Table 1:** Major physical and chemical properties of the biochars examined in this study: C:N,
536 H:C, O:C, and (O+N):C ratios, oxygen functional groups (OFGs), specific surface area (SSA),
537 cation exchange capacity (CEC, calculated from the content of Na, Mg, Al and K) and
538 percentage sorption (%)

539 **Table 2:** Estimated thermodynamic parameters for Pb sorption on Bw, Mw and Ps at 350 ^{o}C and
540 650 ^{o}C

541

Table 1

	Properties (*n*=2)													Sorption (%)			
BC	**Temp. (^oC)**	**Yield (%)**	**Ash (%)**	**C (%)**	**H (%)**	**N (%)**	**S (%)**	**O (%)**	**C:N**	**H:C**	**O:C**	**(O+N)/C**	**SSA ($m^2 g^{-1}$)**	**CEC ($cmol_c kg^{-1}$)**	**pH**	**Pb**	**Cd**	**As**
	350	46.3	4.02	70.1	4.44	0.92	0.13	24.4	88.9	0.76	0.26	0.27	11.40	11.2	9.23	99.7	10.9	37.9
Bw	450	42.3	25.4	76.5	3.63	0.99	0.12	18.8	90.6	0.57	0.18	0.20	10.72	11.5	9.70	99.6	60.8	39.3
	550	34.2	5.80	82.8	2.75	0.90	0.12	13.4	107	0.40	0.12	0.13	17.02	10.1	10.0	99.8	58.1	39.6
	650	28.5	33.1	83.9	1.81	0.89	0.10	13.3	109	0.26	0.12	0.13	17.80	11.7	9.14	99.8	50.9	33.8
	350	37.5	7.52	67.9	4.53	2.16	0.20	25.2	36.7	0.80	0.28	0.31	16.56	23.3	10.2	99.1	62.7	5.32
Mw	450	32.7	7.72	70.8	3.32	1.92	0.15	23.8	43.2	0.56	0.25	0.28	31.45	22.1	11.1	99.3	85.4	0.44
	550	26.2	9.82	77.0	2.41	1.68	0.15	18.8	53.5	0.38	0.18	0.20	58.03	19.0	10.6	99.8	81.2	10.4
	650	22.8	9.77	80.1	1.63	1.58	0.13	16.6	59.3	0.24	0.15	0.17	24.46	21.8	10.6	99.8	88.2	5.52
	350	45.7	7.06	64.3	4.32	1.69	0.32	29.4	44.4	0.81	0.34	0.37	14.03	26.5	10.4	99.6	99.2	28.9
Ps	450	38.1	16.9	70.8	3.18	1.65	0.29	24.1	50.2	0.54	0.26	0.28	14.08	23.7	11.1	99.7	98.4	26.4
	550	32.5	7.14	73.7	2.41	1.58	0.61	21.7	54.6	0.39	0.22	0.24	18.58	19.7	10.6	99.7	96.7	29.2
	650	29.4	24.4	74.6	1.81	1.66	0.26	21.7	52.6	0.29	0.22	0.24	28.11	17.4	10.6	99.7	93.1	27.1

Table 2

Biochar	T (K)	ΔG^o (kJ mol^{-1})	ΔH^o (kJ mol^{-1})	ΔS^o (kJ mol^{-1})
Bw350	298	-2.08	27.75	-0.1
	308	-2.70		
	318	-4.07		
Bw650	298	-5.03	43.2	-0.16
	308	-6.60		
	318	-8.26		
Mw350	298	0.99	19.46	-0.06
	308	-0.01		
	318	-0.26		
Mw650	298	-3.24	44.6	-0.16
	308	-4.02		
	318	-6.43		
Ps350	298	-2.84	18.8	-0.07
	308	-3.71		
	318	-4.29		
Ps650	298	-3.13	6.56	-0.03
	308	-3.94		
	318	-3.79		

Figure 1

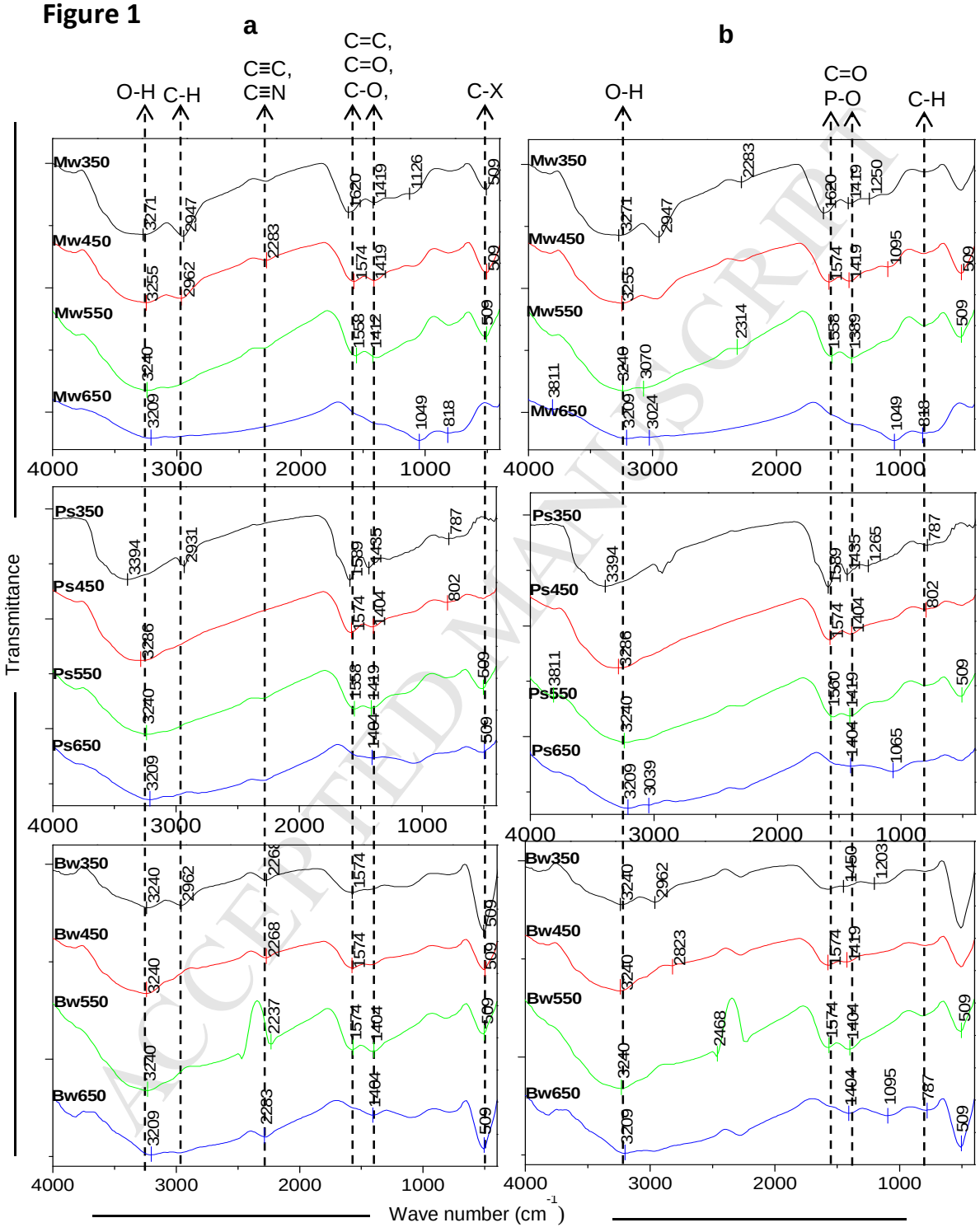
a
b
O-H
C-H
C≡C,
C≡N
C=C,
C=O,
C-O,
C-X
C=O
P-O
Mw350
Mw450
Mw550
Mw650
Ps350
Ps450
Ps550
Ps650
Bw350
Bw450
Bw550
Bw650
Transmittance
Wave number (cm-1)
4000
3000
2000
1000

Figure 2

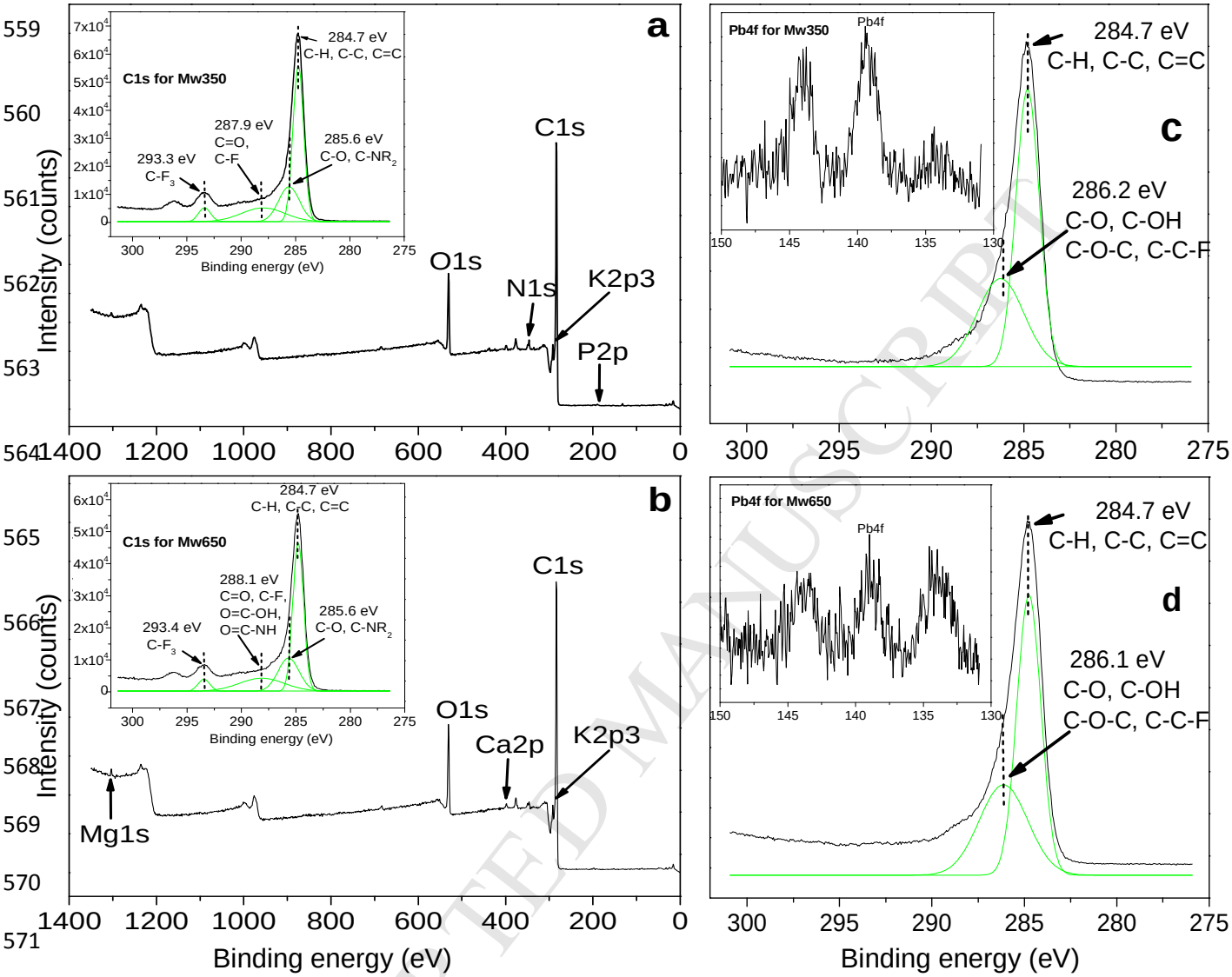

Figure 3

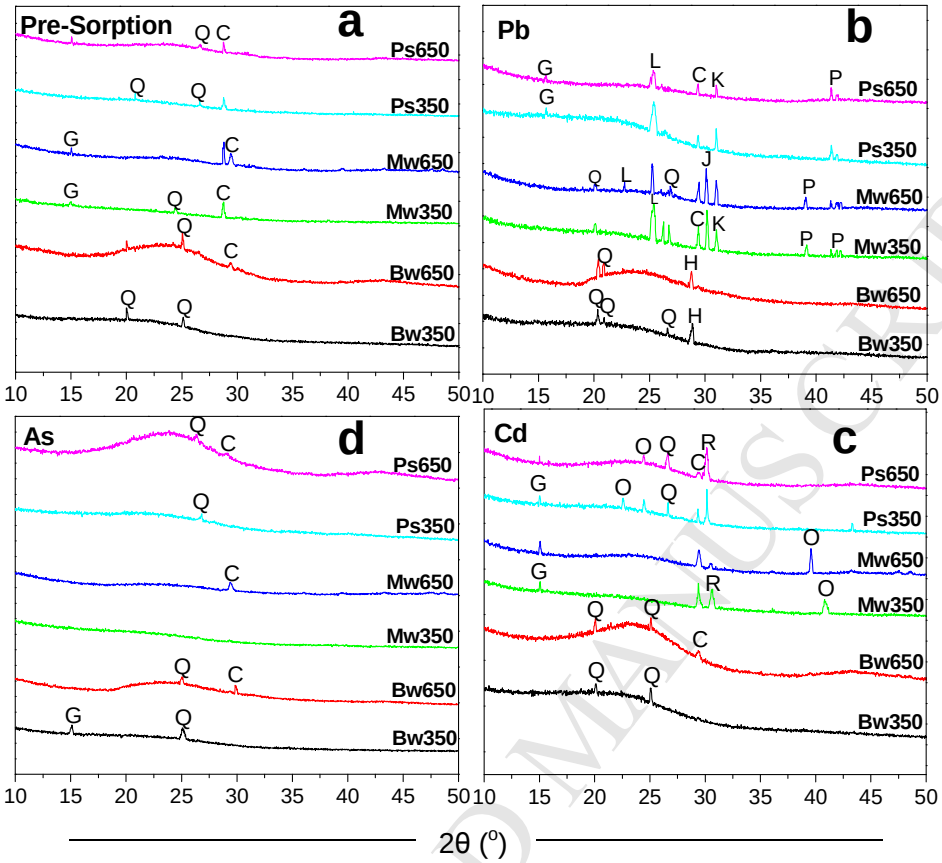

Q=SiO_2, C=$CaCO_3$, **G**= $(Na,Ca)_2(Si)_5O_{10}.3H_20$, **L**=$PbCO_3$, **J**=$Pb_3(PO_4)_2$, **K**=$Pb_9(PO_4)_6$, **P**= $Pb_3(CO_3)_2(OH)_2$, **H**=$PbCO_3(OH)_2$, **O**=$CdCO_3$, **R**=$Cd_9(PO_4)_6$

Figure 4

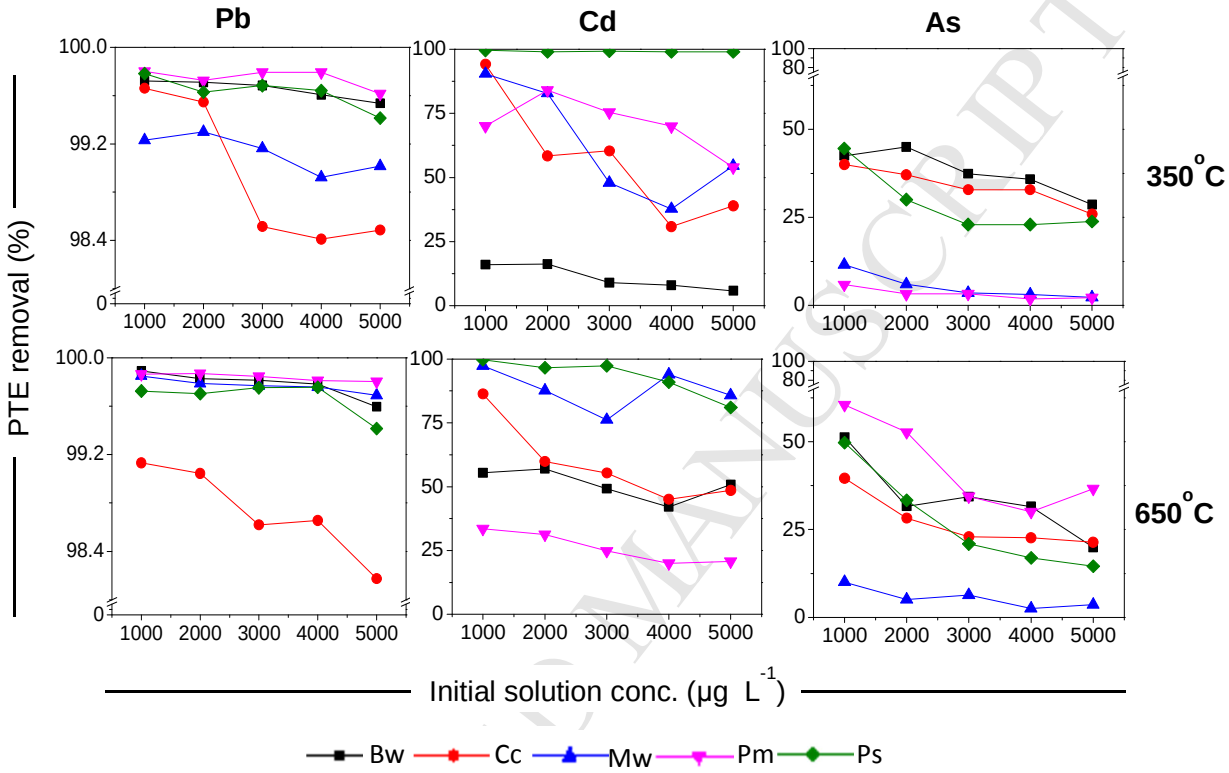

626
627
628
629
630
631
632
633
634
635
636
637
638
639
640
641
642
643
644
645
646
647
648
649
650

Figure 5

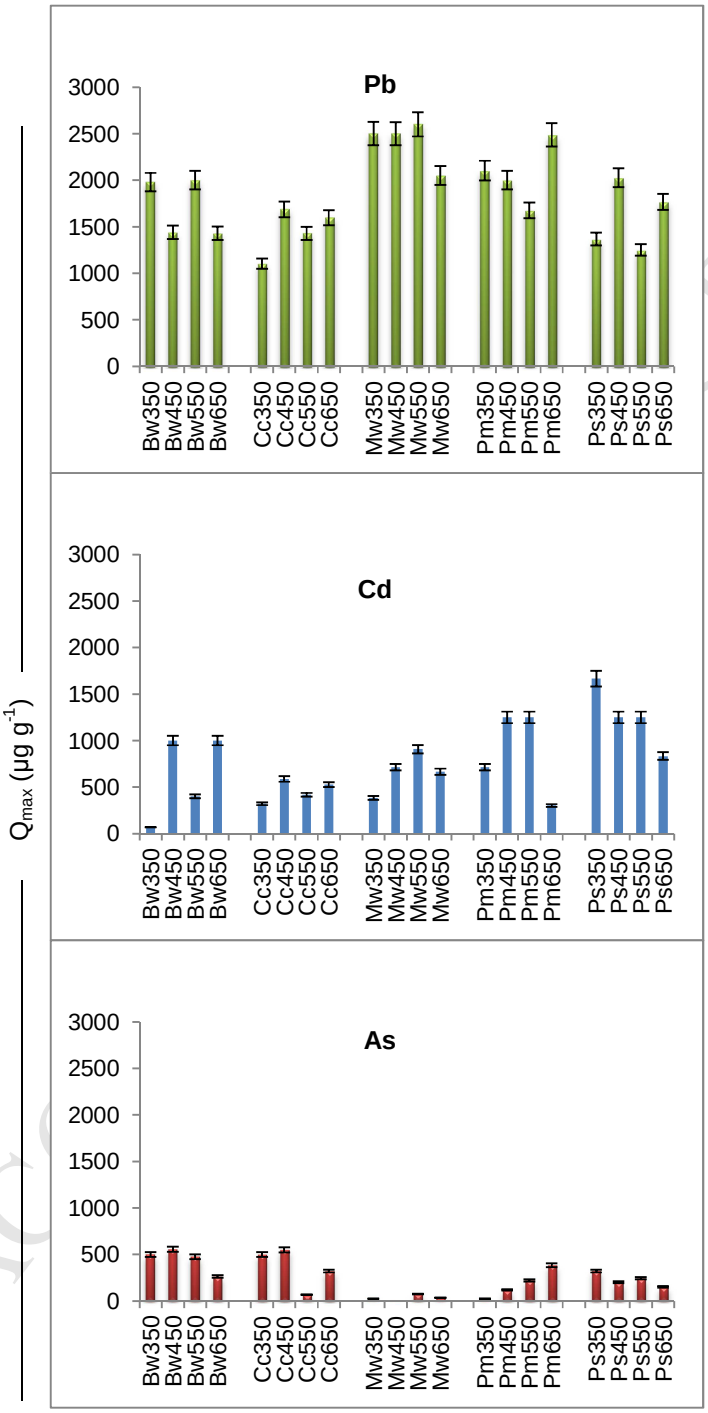

651

652

Figure 6

653

654

655

656

657

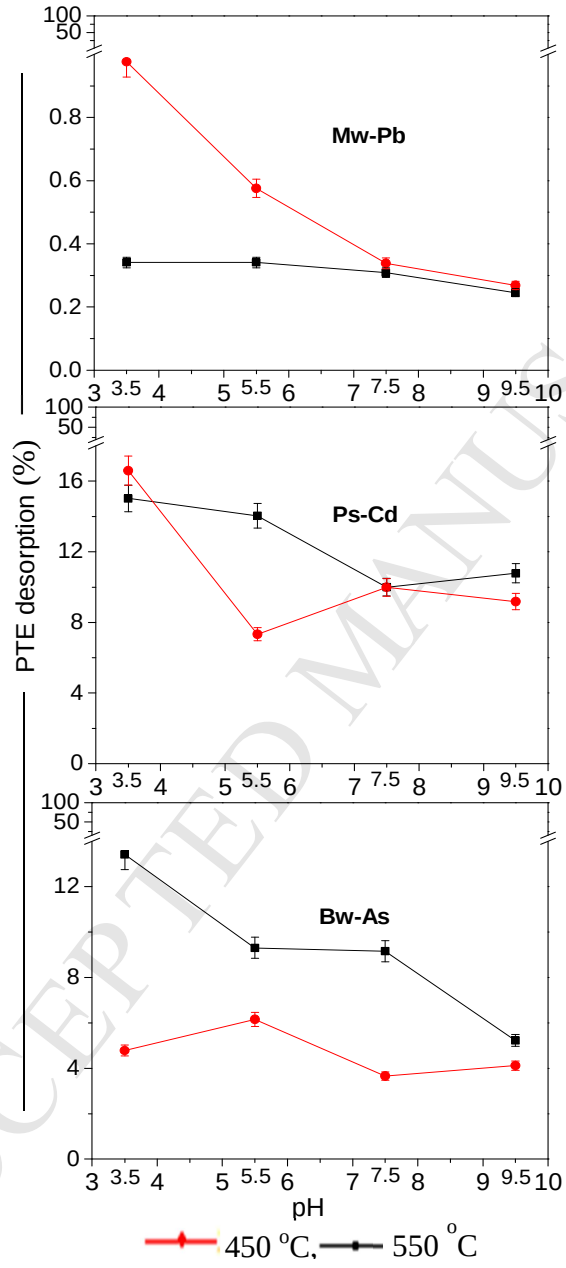

Highlights

- 20 biochars from 5 biomass materials were used for Pb, Cd and As sorption in solution
- Chemical properties (functional groups, ions, minerals) controlled sorption significantly
- The number of mechanisms in sorption processes determine biochar sorption capacity
- The stability of sorbed contaminants on biochar (in soil or water) is pH-dependent
- Understanding biochar properties enhances its engineering for superior sorption qualities